Self-Aggregation of Lipophilic Porphyrins in Reverse Micelles of Aerosol OT

Denisio M. Togashi,*,† Sílvia M. B. Costa,*,† Abílio J. F. N. Sobral,‡ and A. M. d'A. R. Gonsalves‡

Centro de Química Estrutural, Complexo I, Instituto Superior Técnico, 1049-001 Lisbon, Portugal, and Departamento de Química, Universidade de Coimbra, P-3000 Coimbra, Portugal

The aggregation process of *meso*-tetra(4-aminosulfonylphenyl)porphyrin (PC_0), of butyl and dodecyl derivatives (PC_4 and PC_{12}, respectively) in the presence of aerosol-OT (AOT) reversed micelles with different values of $\omega_0 = $ [water]/[AOT] was investigated using steady-state extinction, fluorescence, and resonance light scattering (RLS) techniques. The scattering has been accounted for and the absorption spectra corrected from the extinction spectra. In homogeneous solutions, the porphyrins exist as a monomer showing the Soret band around 420 nm and emission bands at 650 and 716 nm. In reverse micelles, the spectra vary according to the chain length and the amount of solubilized water. Only PC_{12} is dissolved as a monomer at $\omega_0 = 0$, and PC_4 shows some degree of aggregation. PC_0 is present largely as an aggregate. At $\omega_0 \neq 0$, a complete aggregation is observed for PC_4 and PC_{12}, whereas in PC_0, some degree of disaggregation was detected. The extinction spectra of PC_0 and PC_4 in aggregate forms show a broad and red shifted Soret band indicating J aggregates. By contrast, the Soret band intensity of PC_{12} decreases and a new band around 376 nm appears with a broadening of the monomer Soret band which reflects H aggregates. RLS shows a strong signal for PC_{12} at red spectral region at high ω_0 indicating J aggregate types. The fluorescence spectra showed the new band around 670 nm for PC_0 and PC_{12}, whereas in PC_4, only blue shifted bands were observed with ω_0 increase. The global fluorescence quantum yield of the PC_{12} aggregates is lower than the respective monomer. The aggregate sizes were followed by RLS measurements which showed an increase of intensity at around 440 nm. The aggregation dynamics is dependent on both the porphyrin concentration and ω_0.

1. Introduction

Aggregation processes of dye molecules belonging to the class of porphyrins and phthalocyanines have attracted much attention in a wide variety of fields such as photochemistry,[1−23] biochemistry,[4,5] or optical electronics.[6,7] Control of the dye association in a special organized geometry is one of the goals toward improvement of the knowledge of many processes mimetizing light harvesting units in photosynthesis.[8,9] The main criterion for the aggregation process is the type of noncovalent interaction[10,11] that is involved and external effects such as the environment where the processes occur. The balance of these interactions can determine the type of aggregation that the dye can assume in a given supramolecular assembly.[12]

Free base and metalloporphyrins are known to form different aggregates, and the driving forces for these noncovalent molecular complexes can be hydrogen bonds, van der Waals, electrostatic interactions, and the hydrophobic effect.[13] These interactions perform the structural arrangement of monomers such as building blocks for the construction of porphyrin aggregates.[14−17] Therefore, aggregates can be formed through self-assembly in homogeneous solution[18−22] or induced by an association in some heterogeneous media like micelles,[23−27] liposomes[28] or vesicles,[29] proteins,[30] dendrimers,[31] monolayers, or Langmuir−Blodgett films.[32,33]

In the aggregate molecular structure, the monomer molecules are arranged in such way that the transition dipole moments can strongly interact and consequently cause a remarkable change in the electronic spectra of the aggregate. Indeed, in accordance with Kasha's exciton theory,[34] the coupling of the dipole transition moments of monomer molecules, that are aligned parallel ("head-to-tail") to the line joining the molecular centers in the aggregate results in an electronic transition red shifted relative to that of the monomer. These are the features of the J aggregate. On the other hand, the theory anticipates that for the H aggregate the monomer dipole transition moments are perpendicular to the line of centers ("head-to-head") leading to a blue-shift electronic transition relative to the absorption band of the monomer. There is, also, an intermediate case where the transition dipole moments are in skewed arrangements that cause a split in the monomer absorption band resulting in two bands (red and blue shifted) in the aggregate spectrum.

The structural details on how monomer molecules are associated in aggregates cannot be unambiguously characterized only from electronic absorption spectra, because nonspecific aggregates broaden absorption bands. Nevertheless, the aggregates which have been conventionally assigned to J-aggregate (red shift) or H-aggregate (blue shift) types are the two extreme cases which provide some indication of how the monomers are assembled in the aggregate.[18−33]
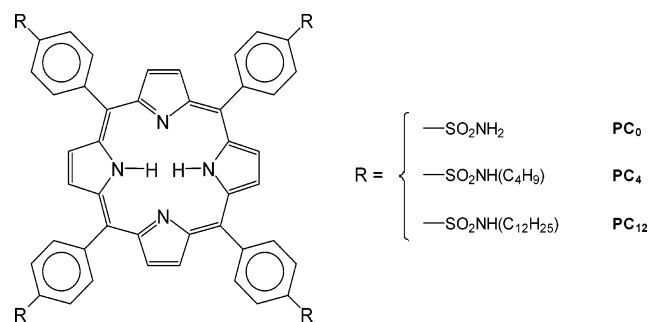
Micelles show great similarity to the cell membrane.[35] These systems are composed of surfactants with polar and nonpolar character which induce self-aggregation to form enormous

* To whom correspondence should be addressed. E-mail: togashi@ist.utl.pt.
† Instituto Superior Técnico.
‡ Universidade de Coimbra.

Self-Aggregation Process of Lipophilic Porphyrins

J. Phys. Chem. B, Vol. 108, No. 31, 2004 **11345**

SCHEME 1

entities (micelles) creating three regions of different polarities: polar, interfacial, and nonpolar regions.

In reverse micelles, the polar solvent is found in the core and thus dispersed in a nonpolar solvent. Water is the polar solvent most used in the reverse micelles,[35] but recently, other polar solvents have been used in these systems.[36,37] The amount of water dissolved in reverse micelles determines most of the physical and chemical properties of the micellar medium.[35,38] Such systems can mimic the water pockets that are often found in membranes. Furthermore, the size of reverse micelles is controlled by the molar ratio of water dissolved to the surfactant concentration (ω_0 = [water]/[AOT]).[35] In general, addition of surfactants at concentrations above the critical micelle concentration (cmc) leads to disaggregation of dye molecules,[23] and sometimes noncovalent interactions between surfactant/dye aggregates can be formed in the premicellar region, i.e., below cmc.[26,39]

In this work, we investigated the uncommon aggregation process of *meso*-tetra (4-aminosulfonyl phenyl) porphyrin derivatives (Scheme 1) in reverse micelles. The sizes, content of water and micelle concentration were varied and the monomer-aggregate spectroscopic properties were followed by means of steady-state extinction (E), emission (EM), and resonance light scattering (RLS) techniques. The recent method[40] to extract the absorption spectra (ABS) from the extinction spectra discounting the scattering contribution has been applied. Preliminary results for the aggregation dynamics of porphyrins in the reverse micelle system are also presented.

2. Experimental Section

2.1. Materials. The porphyrin derivatives, PC_0, PC_4, and PC_{12}, were synthesized and already described.[41] *meso*-Tetraphenyl porphyin (TPP) and sodium 1,4-bis(2-ethylhexyl)sulfosuccinate (AOT) were purchased from Sigma-Aldrich and used as received. All other solvents were spectroscopic grade and used without any further treatment. The water used was previously double distilled.

2.2. Sample Preparation. For the preparation of isooctane/AOT/water reverse micelles, 0.1 M AOT was used for all the porphyrins. Different AOT concentrations (0.001−0.5 M) were used with PC_{12}. From porphyrin stock solutions of chloroform (acetone for PC_0), the appropriate amount was added to an empty volumetric flask and then the solvent was carefully evaporated using a dry nitrogen flow. The porphyrin thin films formed in the flask bottom wall were dissolved with the addition of isooctane/AOT solution. For PC_0 and PC_4, the solutions were sonicated for 15−20 min. The reverse micelles at different molar ratios, ω_0 = [water]/[AOT], were prepared by addition of corresponding water volume to the solution of AOT in isooctane with the porphyrin already incorporated. The solutions were agitated until total transparency was observed and then left at

room temperature overnight before carrying out any measurements. For kinetic traces, the solution of reverse micelle with AOT/isooctane with porphyrin was added to the cuvette and the corresponding amount of water was added. Immediately after the cuvette stirring, the extinction spectra were continuously scanned using time intervals of 5 or 6 min.

2.3. Apparatus. The electronic extinction spectra were recorded with a JASCO V560 UV/vis spectrophotometer with blank correction and the fluorescence spectra with a Perkin-Elmer LS-50B spectrofluorimeter. The instrumental response at each wavelength was corrected by means of a curve provided with the instrument. The resonance light scattering (RLS) spectra were carried out by the simultaneous excitation and emission scanning in right angle geometry. The signal had to be attenuated by a factor of 100 (hundred). All of the RLS spectra were corrected by subtracting the corresponding blank sample. The sample holder of both instruments was thermostated at 25 °C, and all of the measurements were taken using quartz cuvettes with 2 and 10 mm path lengths.

2.4. Methods. The absorption spectra of the aggregates in the micellar system show, in general, appreciable scattering, and therefore, it is more adequate to refer them as extinction spectra. The "true" absorption spectra were extracted from the extinction spectra of samples where RLS spectra show a relevant signal, $I_{RLS}(\lambda)$. Therefore, the absorption spectra were corrected by withdrawing the scattering contribution from the measured optical intensity reduction or total light extinction, $E(\lambda)$,[40a] measured by the spectrophotometer. This correction is made using $E(\lambda)$ = Abs(λ) + $a\,I_{RLS}(\lambda)$ + b. The empirical parameters a and b take into account the monochromator features, detector and the system geometry. The empirical parameters are determined by linear fitting of $E(\lambda)$ vs $I_{RLS}(\lambda)$ in the region where the extinction light observed is only due to the resonance light scattering intensity, i.e., Abs(λ) = 0. This region was 460−490 nm where the correlation coefficients obtained for all of the corrected systems were 0.962 < r <0.987. For a more accurate correction, the methodology developed by Collings et al. could be applied.[40b] However, it requires the determination of the effective path length and then the correction factor for the instruments through standards which are nonabsorbing scatters and nonscattering absorbers. Furthermore polarization effects should also be considered. The fluorescence quantum yields were measured, taking into account the scattering corrections, with 513 nm excitation using TPP in benzene (ϕ = 0.13[42]) as a standard.

3. Results

3.1. Electronic Extinction Spectra. The solvent effect on absorption spectra of porphyrins in solvents has already been studied.[43] In neat solutions, like acetonitrile (Table 1), the spectra show the characteristic features of any porphyrin free base, a D_{2h} symmetry molecule.[44] The ground-state extinction spectra are composed of the Soret (around 415 nm) and four Q-bands (around 513, 546, 590, and 642 nm). It was observed that the Soret band is more sensitive to the solvent polarity showing, in general, a red shift in more polarizable media.[43] However, different trends are observed when the porphyrins are dissolved in isooctane/AOT/water reverse micelles.

All porphyrins are practically insoluble in water and isooctane.[45] However, the solubility of porphyrins is enhanced in the presence of AOT surfactant at a concentration of 0.1 M in the hydrocarbon medium.

At ω_0 = 0, the corresponding Soret band for PC_0 and PC_4 along with the overall spectra are broad reflecting the existence

TABLE 1: Porphyrin Wavelengths (nm) for Extinction (absorption) and Emission Peak Position

porphyrin	medium	extinction (absorption)					emission[a]	
		Soret	Q(1,0)y	Q(0,0)y	Q(1,0)x	Q(0,0)x	(0,0)	(0,1)
	acetonitrile	416.0	514.5	545.0	588.0	641.0	648.5	715.5
	$\omega_0 = 0$	434.5	527.0	560.0	591.0	640.0	649.0[b]/666.0	705.0
	$\omega_0 = 2$	422.0/441.0[b]	526.5	559.0	590.5	641.5	650.5[b]/664.5	710.0
	$\omega_0 = 4$	418.0/439.0[b]	525.0	558.5	590.5	641.0	650.0[b]/665.0	711.5
	$\omega_0 = 6$	418.0/441.0[b]	527.0	559.0	592.5	642.0	650.0[b]/664.0	713.0
PC_0	$\omega_0 = 8$	418.5/440.0[b]	527.0	557.5	591.0	641.0	650.0[b]/663.5	711.0
	$\omega_0 = 10$	418.0/441.5[b]	525.0	559.0	590.0	640.0	650.0[b]/663.0	716.0
	$\omega_0 = 20$	418.0/439.5[b]	524.0	558.5	590.0	638.0	650.0[b]/665.0	708.0
	$\omega_0 = 30$	420.0/436.0[b]	524.0	558.0	589.0	638.5	650.0[b]/666.5	709.5
	$\omega_0 = 40$	418.0/436.0[b]	525.0	558.0	590.0	641.0	650.5[b]/664.5	710.0
	acetonitrile	414.5	511.5	546.0	587.0	642.5	648.5	715.0
	$\omega_0 = 0$	419.0/439.5	521.5	549.0	591.5	641.5	649.0	715.0
	$\omega_0 = 2$	420.0/446.0	523.0	548.5	596.0	642.0	649.0	708.5
	$\omega_0 = 4$	423.0/446.0	523.0	556.0[b]	592.0	640.5	647.0	708.0
	$\omega_0 = 6$	425.0/444.5	524.0	553.0[b]	594.5	641.5	644.5	708.0
PC_4	$\omega_0 = 8$	425.0/446.0	523.0	554.0[b]	591.5	642.0	643.5	708.0
	$\omega_0 = 10$	426.0/444.0	523.0	555.0[b]	592.0	642.0	643.0	707.0
	$\omega_0 = 20$	441.0	521.0	553.0[b]	590.0	641.0	643.0	707.0
	$\omega_0 = 30$	441.0	522.0	554.0[b]	592.0	642.0	644.0	708.0
	$\omega_0 = 40$	439.5	521.0	550.0[b]	592.0	642.0	643.0	708.0
	acetonitrile	415.5	513.0	547.0	588.5	643.5	649.5	715.5
	$\omega_0 = 0$	420.0	516.0	549.0	590.5	647.0	650.0	717.0
	$\omega_0 = 2$	419.5	515.5	550.0	590.5	646.5	649.5	718.0
	$\omega_0 = 4$	419.0	515.5	549.5	589.5	646.5	650.0	716.0
PC_{12}	$\omega_0 = 6$	373.0/419.0	517.5	548.0	589.5	646.5	651.0[b]/664.0	717.5
	$\omega_0 = 8$	376.0/419.0	519.0	550.0	590.5	646.5	649.5[b]/670.0	717.5
	$\omega_0 = 10$	379.0/419.0	520.5	549.0	592.0	645.5	650.0[b]/670.5	716.5
	$\omega_0 = 20$	377.0/421.5	519.0	551.0	588.0	645.5	650.0[b]/671.0	715.0
	$\omega_0 = 30$	375.5/421.5	519.0	550.0	589.0	645.5	651.0[b]/671.5	717.5
	$\omega_0 = 40$	376.0/421.5	518.5	550.0	589.5	646.0	651.0[b]/671.0	715.0

[a] Excitation at Q(1,0)y band. [b] Shoulder.

of large aggregates in the solution. This is shown in Figure 1, parts a and b, for PC_0 and PC_4 $\omega_0 = 0$ solutions (spectra 1 in both) whose extinction extends beyond 700 nm whereas, in acetonitrile solutions PC_0 and PC_4, no extinction at this wavelength is detected. Indeed, with the naked eye, a slight turbidity of the solutions may be noted. A significant modification in the porphyrins' Soret band shape is observed, as ω_0 is increased. In PC_0, the extinction band in the Soret region at $\omega_0 = 0$ (Figure 1a, spectrum 1) is very broad, with the full-width half-maximum (fwhm) value about 5590 cm^{-1} and a red shift of 18 nm as compared to the corresponding Soret band in acetonitrile (Table 1). When the water concentration is increased, the Soret band becomes narrow (fwhm ~ 3360 cm^{-1}, at $\omega_0 = 40$) and a new band located at 418 nm is revealed (Figure 1a, spectrum 4). Almost no changes were observed in the Q-bands. Although no clear isosbestic points were observed, the extinction ratios between 418 and 434.5 nm show a trend when correlated to ω_0. There is a gradual increase in the ratio from $\omega_0 = 0$ to 8, and beyond this, no further changes were observed for further water additions (until $\omega_0 = 40$).

A continuous decrease and broadening of the extinction bands of PC_4 and PC_{12} were observed with increase of ω_0. For PC_4 at $\omega_0 = 0$ (Figure 1b, spectrum 1), the Soret band shoulder observed in PC_0 is changed into a peak with extinction at around 440 nm and a sharp peak with the maximum located around 420 nm (fwhm ~ 1100 cm^{-1}). Apart from the extinction at 440 nm, a broad base and small red shift, the Soret band profile for PC_4 is similar to the one observed in acetonitrile solution. Contrary to PC_0, the ratio between the two extinction bands at 420 and 440 nm of PC_4 undergoes a continuous decrease with ω_0. However, similarly to PC_0, no significant changes were accounted for $\omega_0 > 8$.

The monomer extinction band of PC_{12} is clearly observed at $\omega_0 = 0$ (Figure 1c, spectrum 1). The full spectrum profile is similar to the absorption spectrum in acetonitrile. The PC_{12} Soret band is only 4.5 nm red shifted by comparison to that in acetonitrile (Table 1). However, by contrast to PC_4, the addition of water affects the intensity of the Soret band which decreases and shifts slightly to the red region in the spectra. Another effect is the appearance of a new blue shifted band at 374 nm which increases with ω_0. The Q-band locations are practically unaffected by additional water. Moreover, the red-edge extinction that extends to 460 nm is observed at $\omega_0 \neq 0$ (Figure 1c, spectra 2−4).

At high values of ω_0, a skewed baseline in the PC_{12} extinction spectra is observed (see the amplification of Q-bands region in Figure 1c). If the features observed in the PC_{12} Soret band at $\omega_0 = 0$ correspond to the presence of monomer, the reduction of light extinction intensity in the Soret band and the tail of the baseline with increasing water concentration mean that, in reverse micelles, the formation of larger aggregates probably occurs at the monomer's expense.

3.2. Emission Spectra. The fluorescence spectra are weakly affected by the medium polarity.[43] In acetonitrile solutions, PC_0, PC_4, and PC_{12} show two bands around 650 and 717 nm, named Q(0,0) and Q(0,1), respectively (Table 1). Similar monomer spectra are observed for PC_4 and PC_{12} at $\omega_0 = 0$ upon Q-band excitation (spectra 1 in Figure 2b,c). By contrast, for PC_0, these similarities were observed only at 417 nm excitation.

A new band appears around 670 nm for PC_0 and PC_{12} when $\omega_0 \neq 0$ and the emission spectra become dependent on the excitation wavelength for all of the porphyrins. This can be observed mainly in the PC_0 fluorescence spectra at $\omega_0 = 40$ solutions (Figure 2a). Spectrum 2 for PC_0 collected at 513 nm excitation is quite different from spectrum 3 (at 439 nm excitation). No isoemissive points were detected for any porphyrin. When the solution is excited in the Q-band region (513 nm), the intensity ratio between the 650 and 670 nm bands
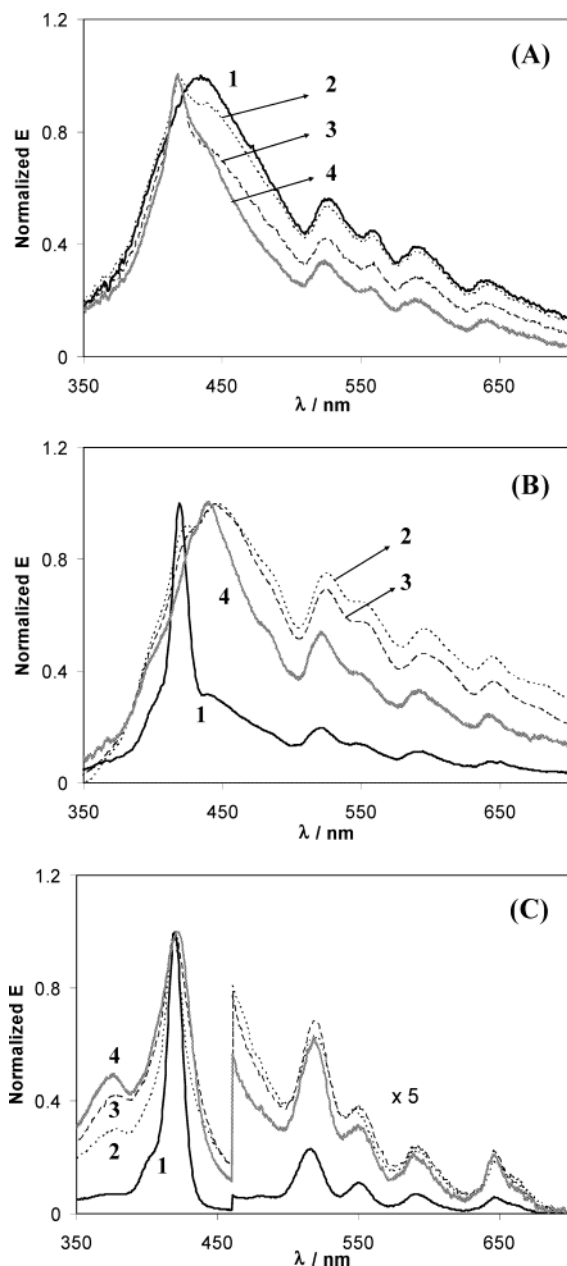
Self-Aggregation Process of Lipophilic Porphyrins

J. Phys. Chem. B, Vol. 108, No. 31, 2004 **11347**

Figure 1. Electronic extinction spectra of PC_0 (A), PC_4 (B), and PC_{12} (C) in AOT reverse micelles at different ω_0 values. 1, $\omega_0 = 0$; 2, $\omega_0 = 4$ (except for PC_{12} where $\omega_0 = 6$); 3, $\omega_0 = 10$; 4, $\omega_0 = 40$.

Figure 2. Fluorescence spectra of porphyrins in AOT reverse micelles. PC_0 (A): 1, $\omega_0 = 0$ excited at 513 nm; 2, $\omega_0 = 40$ excited at 513 nm; 3, $\omega_0 = 40$ excited at 439 nm. PC_4 (B): 1, $\omega_0 = 0$ excited at 513 nm; 2, $\omega_0 = 40$ excited at 513 nm; 3, $\omega_0 = 40$ excited at 439 nm. PC_{12} (C): 1, $\omega_0 = 0$ excited at 513 nm; 2, $\omega_0 = 40$ excited at 513 nm. 3, $\omega_0 = 40$ excited at 374 nm.

(i.e., I_{650}/I_{670}) experiences an increase from $\omega_0 = 0$ until approximately $\omega_0 = 10$. With further water additions, a plateau is achieved which remains unchanged until $\omega_0 = 40$. When the emission spectrum is scanned at an excitation wavelength where the porphyrin aggregates absorb mostly, e.g., 439 nm at $\omega_0 = 0$, the I_{650}/I_{670} is lower than the ratio of the same bands generated by excitation wavelength where the monomer mainly absorbs (i.e., at 417 nm). If the new band ($\sim$670 nm) represents the fluorescence of aggregates and the usual band at 650 nm is associated with the presence of monomers, then the monomer concentration rises when the emission intensity at 650 nm increases with solubilization of water molecules. The opposite effect is observed for PC_{12} fluorescence emission. Increasing ω_0 leads to a gradual reduction of the 650 nm band intensity and the increase of the 670 nm band intensity for PC_{12}. At $\omega_0 = 40$, the PC_{12} fluorescence spectra upon 374 nm excitation has a maximum intensity at 670 nm (Figure 2c, spectrum 3). Also, the I_{650}/I_{670} value for spectrum 3 is close to that obtained
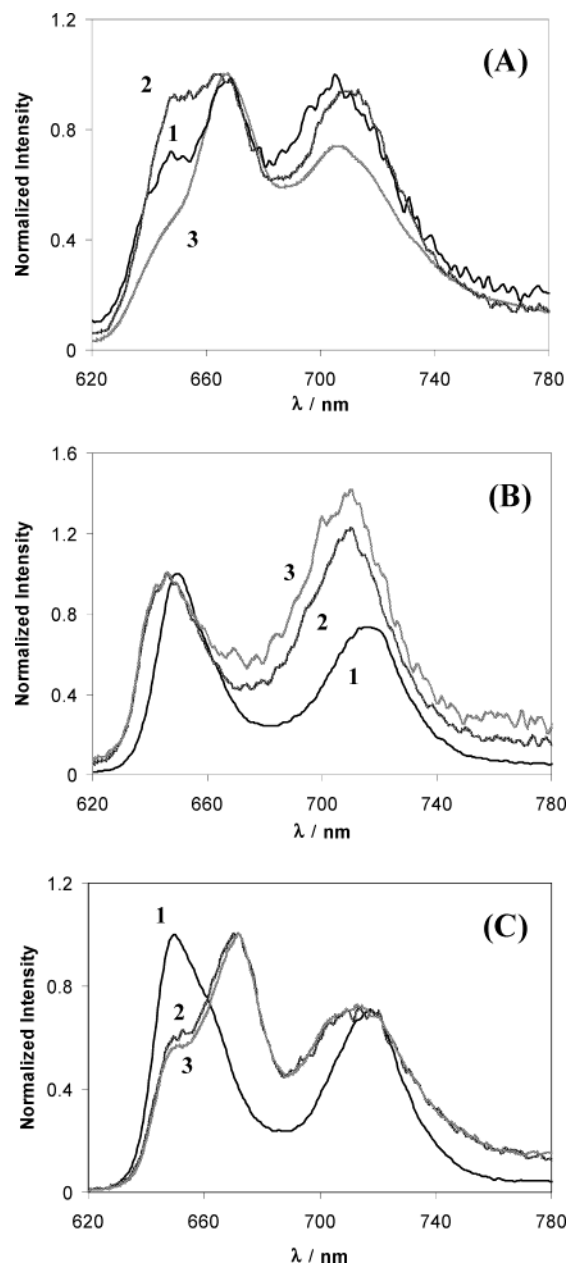
for spectrum 2, which was obtained using an excitation in the Q-band.

The water molecules dissolved in the reverse micelle cause a blue shift to the PC_4 emission Q-bands, from 649 and 713 nm (Figure 2b, spectrum 1) to 644 and 709.5 nm (Figure 2b, spectrum 2) and a decrease of Q(0,0) band intensity by comparison to the Q(0,1) intensity, instead of showing any emission band around 670 nm. To be exact, the ratio between Q(0,0) and Q(0,1) intensities is reduced when the ω_0 is increased until $\omega_0 = 8$. Above this value, the ratio is almost unchanged.

3.3. Fluorescence Excitation Spectra. The aggregates can also be followed by steady-state fluorescence excitation spectra. Figure 3 shows changes in the excitation spectra of PC_0, PC_4, and PC_{12} in reverse micelles at different ω_0 and emission wavelengths.
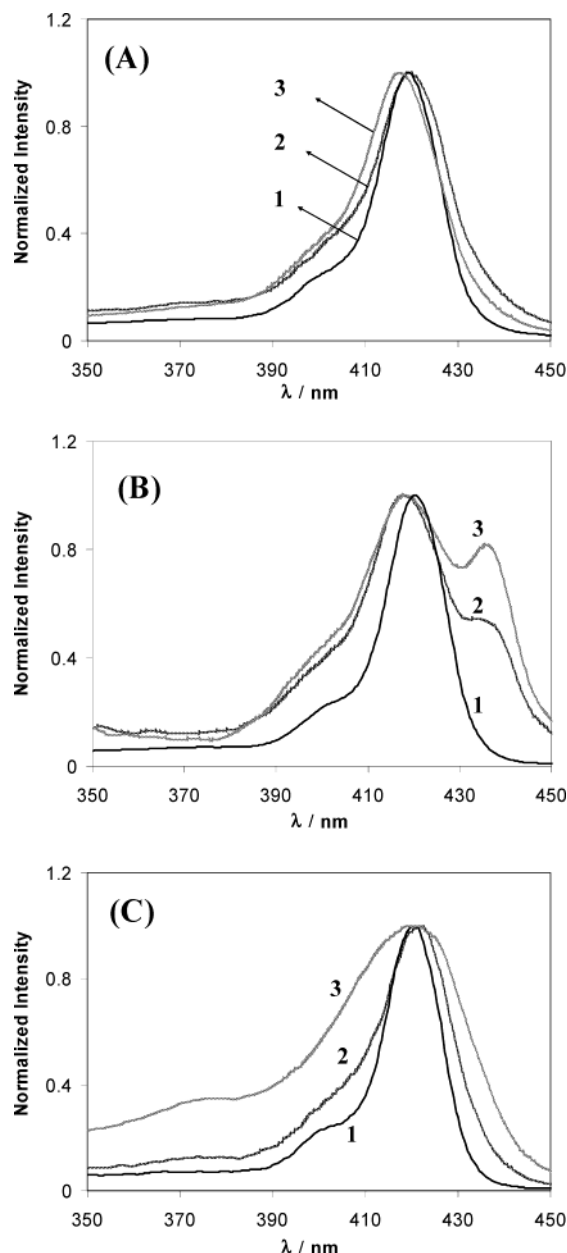
Figure 3. Fluorescence excitation spectra of porphyrins in AOT reverse micelles. PC_0 (A): 1, $\omega_0 = 0$ with emission at 650 nm; 2, $\omega_0 = 0$ with emission at 670 nm; 3, $\omega_0 = 40$ with emission at 670 nm. PC_4 (B): 1, $\omega_0 = 0$ with emission at 650 nm; 2, $\omega_0 = 40$ with emission at 650 nm; 3, $\omega_0 = 40$ with emission at 640 nm. PC_{12} (C): 1, $\omega_0 = 0$ with emission at 650 nm; 2, $\omega_0 = 0$ with emission at 670 nm; 3, $\omega_0 = 40$ with emission at 670 nm.

The excitation spectra collected using the emission at 650 nm for porphyrins at different ω_0 solutions (Figure 3, all spectra 1) are more akin to the corresponding absorption spectra in pure solvents. These features are almost unchanged with ω_0. On the other hand, the excitation spectra for emission at 670 nm in $\omega_0 = 0$ solutions are broad in the Soret region (spectra 2 in Figure 3, parts a and c) but still narrow by comparison to the corresponding extinction spectra (Figure 1). This suggests that some of the nonspecific aggregates either absorb or scatter in the Soret band region and do not fluoresce. The normalized excitation spectra for PC_4 in $\omega_0 = 0$ solution scanned at 642 or 670 nm are similar to those scanned at 650 nm. Blue shifts and broadening are observed in the excitation spectra of PC_0 and PC_4 when ω_0 is increased, as it is observed in Figure 3a for spectra 2 and 3, and in Figure 3b for spectra 1 and 2. In the
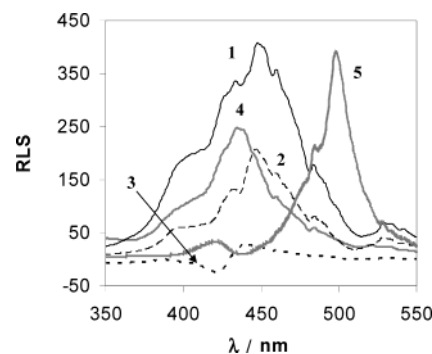

Figure 4. Resonance light scattering of porphyrins in AOT reverse micelles. PC_0 (1), PC_4 (2), and PC_{12} (3) in $\omega_0 = 0$. PC_{12} in $\omega_0 = 40$ (4) and TSPP (5) in water (see text).

case of PC_4, a new prominent band is observed in the excitation. This band with the maximum at 436 nm in spectra 2 and 3 in Figure 3b may correspond to the 440 nm band observed in the extinction spectra at high ω_0 (Figure 1b, spectrum 4). In addition, the intensity at 436 nm in the excitation spectra increases when the probe emission wavelength is varied from 650 to 640 nm for the $\omega_0 = 40$ solutions (Figure 3b, spectra 2 and 3).

The excitation spectra of PC_{12} collected using the emission at 670 nm show remarkable changes with ω_0 (Figure 3c, spectra 2 and 3). At low ω_0, the excitation spectrum 2 is close to the excitation spectrum 1 (emission at 650 nm). When ω_0 is increased, the corresponding Soret band becomes broad and the red-edge increasing signal extends beyond 450 nm and the signal grows at 350−390 nm. The excitation spectrum of PC_{12} at $\omega_0 = 40$ collected using the emission at around 670 nm (Figure 3c, spectrum 3) is quite similar to the extinction spectrum at $\omega_0 = 40$ (Figure 1c, curve 4).

3.4. Resonance Light Scattering Spectra. Recently, Pasternack et al. developed a new technique which uses a conventional spectrofluorimeter to measure the resonance light scattering of supramolecular systems and therefore applied it to study the presence and size of large aggregates.[16,21,24,40,46] The technique is extremely dependent on aggregate size and consists of light scattering enhancement at right angle geometry between excitation and emission beams. The RLS intensity is high at regions where there is an electronic extinction. When the light is absorbed by a polarizable particle, a larger oscillation is induced and therefore this particle "emits" the absorbed light.

Porphyrin aggregates formed in the AOT reverse micelle were observed using this technique. The well-known RLS spectrum of the tetrakis(4-sulfonatophenyl) porphyrin J aggregates was obtained (Figure 4, spectrum 5). This type of aggregate shows a scattered light signal around 490 nm[40b,46] and can have a hydrodynamic diameter around 0.2 μm composed of more than 100 000 aggregated porphyrins. Moreover, the RLS spectrum 5 is sharp as a result of strong electronic coupling between the transition dipole moments of the porphyrin monomers.[46]

Large signals were found for PC_0 and PC_4 at $\omega_0 = 0$ (Figure 4, spectra 1 and 2) with maxima around 449 nm. These porphyrin aggregates experience a slight reduction in the light scattering intensity when ω_0 is increased. This reflects some reduction in the size or concentration of the large aggregates. The maxima of RLS spectra change slightly with ω_0. Thus, the RLS signal corroborates the presence of larger aggregates, probably colloidal sized, for the porphyrins PC_0 and PC_4 in the ω_0 range studied. Furthermore, the RLS spectra for PC_0 (mainly) and PC_4 are broader than the spectrum 5. This can imply that

Self-Aggregation Process of Lipophilic Porphyrins

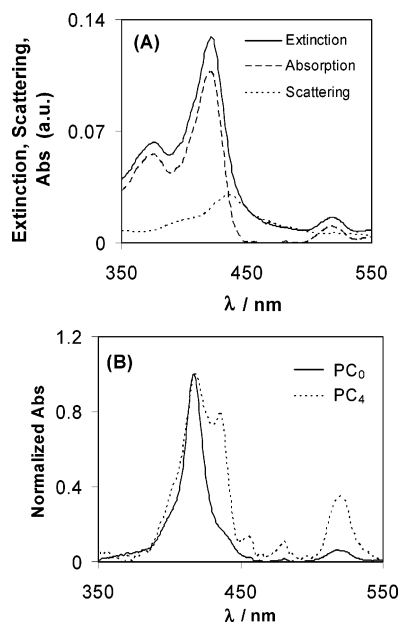*J. Phys. Chem. B, Vol. 108, No. 31, 2004* **11349**

Figure 5. Electronic absorption spectra extracted from the extinction spectra and scattering for PC_{12} (A) and PC_0 and PC_4 (B) in $\omega_0 = 40$.

the bands in RLS spectra for PC_0 and PC_4 are overlapped with a broad nonresonance light scattering.

Spectrum 3 of PC_{12} in $\omega_0 = 0$ solution (Figure 4) shows the absence of large aggregates in solution, i.e., spectrum 3 shows an absorption of light mainly around 420 nm. By contrast, the addition of water gives an increase in intensity at 436 nm shown in spectrum 4, Figure 4. The highest intensity is achieved around $\omega_0 = 10$ after which, the intensity does not change appreciably.

3.5. Absorption Contribution from Extinction Spectra. The extinction spectra obtained from the spectrophotometer for the samples where the resonance light scattering were observed contain some contribution of scatters that can make them very different to absorption spectra profile, i.e., the absorption bands maxima may be different from the extinction bands observed in those system with scattering contribution. Therefore, the spectral corrections were performed following the method described in the experimental part.

Figure 5a shows the results obtained from separation into absorption and scattering contributions in the extinction spectrum using the RLS spectrum of PC_{12} in $\omega_0 = 40$. It is observed that the absorption spectrum is mainly different from the extinction in two points: the intensity and the red-edge at around 460 nm. The band at the blue region side of the Soret is still present and basically no shifts are observed. For the other porphyrins, the absorption spectra extracted from the extinction spectra show a more different profile. A much skewed absorption spectra were observed after the correction of the other porphyrins and then an empirical treatment (subtracting the straight line connecting the extremes of the spectrum) to correct the baseline. This allows the assignment of the peak positions but not the absorption values.

The absorption spectrum of PC_0 in $\omega_0 = 40$, in Figure 5b, is sharper than the extinction spectrum observed in Figure 1a. The more interesting thing is that this spectrum is similar to the absorption spectra in neat solutions[43] but like in the extinction spectra, there is a broader base where a shoulder around 440 nm is still observed. The PC_4 absorption spectrum in $\omega_0 = 40$ in Figure 5b shows some similarity when compared to the extinction spectrum in Figure 1b. The maxima bands are almost the same. However, in the corrected spectrum, the absorption at 419 nm is more prominent than the absorption at 436 nm.

The opposite happens in the extinction spectrum where the peak at 419 nm is covered by the broad band. However, this peak is better observed at the excitation fluorescence spectrum in Figure 3b. In fact, the corrected absorption spectrum of PC_4 in $\omega_0 = 40$ is very similar to the excitation fluorescence spectrum in Figure 3b. Again a very sharp absorption band on Soret region and the peak at 436 nm are observed. Also, a shoulder around 400 nm is observed. Furthermore, an intensification of the Q-band at 520 nm is another feature that can be observed on the absorption spectrum of PC_4 in $\omega_0 = 40$.

3.6. Global Fluorescence Quantum Yields. The aggregated compounds normally show weak emission or exhibit lower fluorescence quantum yields than the monomer, due to nonradiative decay efficiency. In the presence of micelles or reverse micelles, the aggregates can normally be disrupted to their monomeric forms. This process can also be followed by changes in fluorescence quantum yield.[25,28]

The fluorescence quantum yields of porphyrins in the presence of aggregates in the micellar system are not easy to evaluate due to unknown concentrations of fluorescent species and the scattered light. Therefore, we obtained the overall fluorescence quantum yields when the scattered light intensity observed at excitation wavelength was not high and the correction from resonance light scattering could be performed. This happens for PC_{12} fluorescence quantum yields at $\omega_0 > 4$, where 43% of observed extinction on average was caused by resonance light scattering at excitation light. The emission efficiency of PC_0 and PC_4 were not considered. In these porphyrins, the corrected absorption spectra showed strong sloping baselines as pointed before. Furthermore, such extinction spectral features observed for those porphyrins reveal the contribution of large entities (particle sizes greater than incident wavelength light) which may cause a strong coupling between the spatial contribution and the wavelength dependence part in the scattering amplitude thus, making the applied correction difficult.[40a]

The spectral properties show that the PC_{12} monomer is the major species in AOT solution in isooctane. PC_{12} fluorescence emission efficiency in $\omega_0 = 0$ solution and in acetonitrile have nearly the same value (0.16). The fact that these values are similar corroborate that PC_{12} is dispersed into reverse micelles as a monomer which is in agreement with the RLS spectra at $\omega_0 = 0$ solution, where no large aggregates were detected (no scattering light correction was needed). When water is added, there is a narrow range where the total fluorescence quantum yield practically does not change ($\omega_0 \leq 4$), and then, the total quantum yield decreases gradually until approximately 0.1 at $\omega_0 = 40$. Such reduction of fluorescence efficiency indicates that there is a contribution of species with fluorescence quantum yield lower than the fluorescence quantum yield of monomer upon water addition.

3.7. AOT Concentration Effect on Electronic Absorption and RLS Spectra. The presence of AOT surfactant affects the spectroscopic properties of long alkyl chain PC_{12} porphyrin. In this experiment, the absorption spectra are extracted from the extinction and RLS spectra. The result may be seen in Figure 6 where PC_{12} spectra normalized at Soret absorption band are shown at different AOT concentrations (from 0.001 to 0.5 M) in isooctane solution, i.e., $\omega_0 = 0$.

The PC_{12} absorption spectra for low AOT concentrations are quite similar to those observed at high values of ω_0 (see Figure 1c, curve 4). The Soret band split into two around 376 and 421 nm is also observed at low AOT concentration for PC_{12} in ω_0
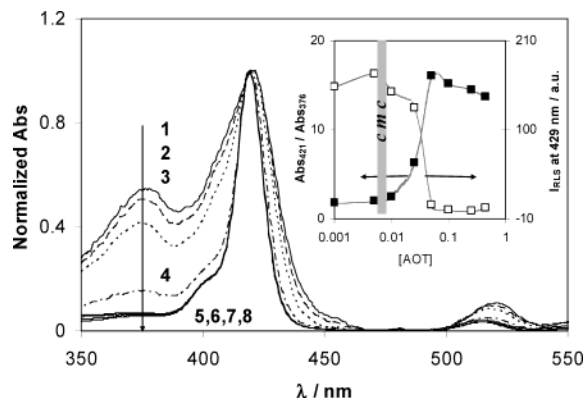
Figure 6. Electronic absorption spectra normalized at Soret maximum band for PC_{12} in increasing AOT concentration: 1, 10^{-3} M; 2, 5×10^{-3} M; 3, 10^{-2} M; 4, 2.5×10^{-2} M; 5, 5×10^{-2} M; 6, 0.1 M; 7, 0.25 M; 8, 0.44 M. Inset: On the left, it is the variation of absorption band ratio between 421 and 376 nm of PC_{12} in isooctane with AOT concentration. On the right is the variation of RLS signal of PC_{12} in isooctane with AOT concentration.

$\omega_0 = 0$ solutions. Furthermore, the red-edge of the 421 nm absorption band, the general red shift, and intensification of Q-bands may be seen.

Both absorption bands in the Soret region fade away when the surfactant concentration is a little above the cmc ($(0.3-3) \times 10^{-3}$ M).[47] When the AOT concentration is much above the cmc, the typical monomer Soret band is observed, similar to the one observed for $\omega_0 = 0$ (Figure 1c, curve 1).

The solubility of PC_{12} porphyrin in isooctane is very low but a small RLS signal was observed which could mean the presence of large aggregates in low concentration. In the presence of 0.001 M AOT, there is an improvement in the PC_{12} solubility and also an increase in RLS intensity. Apparently, there is a noncovalent interaction between the AOT surfactant and the PC_{12} porphyrin. This interaction seems to help the formation of large aggregates such as those obtained in the micellar system at high ω_0.

The insert of Figure 6 displays features from both spectroscopic methods: the ratio of 421 and 376 nm absorption bands and the intensity of RLS spectra at 429 nm. The large aggregate contribution to the absorption and RLS spectra is reduced with increasing AOT concentration until no more detectable changes are observed which happens much above the cmc, namely above 0.05 M of AOT.

The effect of AOT concentration in the presence of water on PC_{12} aggregation was also observed. Using a constant concentration ratio [water]/[AOT] = 10, the concentration of AOT was changed from 0.01 to 0.50 M. Once more, the same trend was observed for the experiment in the absence of water, as shown in Figure 6. At low AOT concentration (0.01 M), the extinction (absorption) and fluorescence spectra are the same as those observed at high water concentration at [AOT] = 0.1 M, i.e., the Soret band corresponding to the PC_{12} monomer shows the split and the fluorescence spectrum shows the presence of the 670 nm band. As the surfactant concentration increases the monomer features in the extinction (absorption) and fluorescence spectra become evident. No changes were observed from [AOT] $\geq$ 0.30 M at [water]/[AOT] = 10.

3.8. Aggregation Kinetics of Porphyrins in the Reverse Micelles. The kinetics of porphyrin PC_{12} aggregation in the isooctane/AOT/water micelles was studied by following the monomer concentration via the Soret band maximum depletion. In this experiment, it was not possible to follow simultaneously the RLS signal and therefore to obtain changes in the "true"

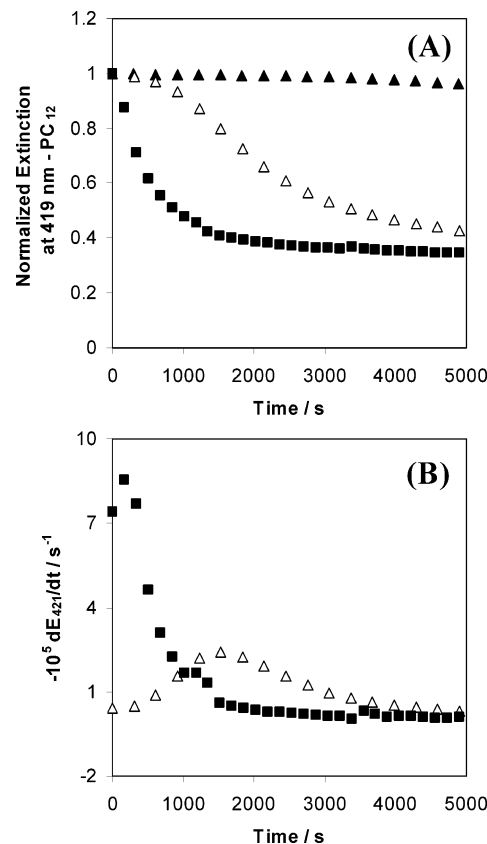

Figure 7. (A) Aggregation kinetic traces normalized at $t = 0$ of 1.5 μM PC_{12} in $\omega_0 = 5$ (▲) and $\omega_0 = 10$ (■) and 3.0 μM PC_{12} in $\omega_0 = 5$ (△). (B) Variation of Soret extinction with time for 3.0 μM PC_{12} in $\omega_0 = 5$ (▲) and 1.5 μM PC_{12} in $\omega_0 = 10$ (■).
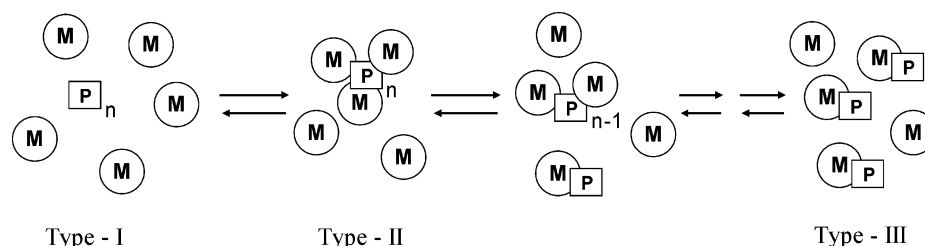
absorption. A clear picture of the porphyrin concentration effect on the aggregation rate is observed at $\omega_0 = 5$ (Figure 7a). For 1.5 μM PC_{12} ($\omega_0 = 5$), practically no changes are observed on the Soret extinction band maximum during the time scale of the experiment. On the other hand, the rate of the aggregation increases when the concentration of PC_{12} porphyrin is 2-fold ($\omega_0 = 5$).

Besides the initial porphyrin concentration, the effect of the amount of water on the porphyrin aggregation kinetics is also important as can be seen in Figure 7a. In fact, the aggregation process is faster at $\omega_0 = 10$ than at $\omega_0 = 5$ where, in both systems, PC_{12} is present at the same concentration. The water/ AOT molar ratio effect on the aggregation process was also observed for PC_4, and it had similar effects, though less pronounced than those observed for PC_{12}.

Three stages can be distinguished in the rate variation from time traces for the aggregation of 3.0 μM PC_{12} in solution of $\omega_0 = 5$ (Figure 7b, open triangles). In the first stage, a time interval around ~600 s, the aggregation process is very slow. After this interval, the porphyrin monomer consumption rate grows until it achieves a maximum value at around 1500 s. In the second stage, the process slows down until it reaches the last stage where the system seems to be in equilibrium. In summary, the rate of reduction in porphyrin monomer concentration assumes a "bell shape" as in time progresses. Similar three stages were also observed by other authors for aggregation of tetrakis(4-sulfonatophenyl) porphyrin.[65]

The ill defined "bell shape" for the PC_{12} rate of concentration variation with time is observed, when the amount of water is 2-fold, i.e., in solution of $\omega_0 = 10$ (Figure 7b, square symbol). In this case however, the shape is narrow and the maximum

Self-Aggregation Process of Lipophilic Porphyrins

J. Phys. Chem. B, Vol. 108, No. 31, 2004 **11351**

SCHEME 2

Type - I   Type - II   Type - III

rate is almost 10 times greater than for the $\omega_0 = 5$ micellar system. Additionally, the maximum of the "bell shape" for $\omega_0 = 10$ corresponds to 170 s (from $t = 0$ s) and is nearest to the initial time of the process.

The monomer behavior of nonsubstituted porphyrin, PC_0, is different from the other two alkyl-substituted porphyrins. However, it is important to state that, due to the presence of large aggregates of this porphyrin, the baseline of the full corrected extinction spectra is distorted as above-mentioned. The kinetic traces obtained, also demonstrate this feature, i.e., the light extinction decreases at 700 nm with time. This is an indication that some precipitation of large aggregates may occur in a parallel process. It was noted (extinction decreasing at 700 nm) that the precipitation occurred but very slowly even in $\omega_0 = 0$ and improves in the presence of water ($\omega_0 \neq 0$). The same behavior was observed for PC_4 but not for PC_{12}. To avoid precipitation, much diluted concentrations were used. However, besides very low extinction signals in the probe region (monomer Soret maximum band), a small variation in the optical density (some lower than 5%) was observed during the experimental time scale. Even under these tough conditions, the dynamic process involving the PC_0 in reverse micelle is opposite to that observed for PC_4 and PC_{12} porphyrins.

As mentioned above, it looks like that there are large aggregates of PC_0 present in reverse micelles. The measurement of Soret maximum band for PC_0 showed an increase in light extinction, which points toward either an increase of monomer concentration or on higher scattering in the presence of isooctane/AOT/ water micelles. Since the extinction decreases at 700 nm, it looks that an increased on monomer concentration is more likely. Besides the appearance of monomers, the rate for the reaction decreases when the ratio [water]/[AOT] increases. By contrast to PC_{12}, the porphyrin PC_0 in reverse micelles shows two different regions (not shown): the first region is a very fast growth (time < 1 s) for which our measurement procedure was inadequate and the second region where the reaction rate slows down until no more changes are observed in the maximum absorption for the PC_0 monomer (~417 nm). Also the overall growth rate for the PC_0 monomer is affected by the amount of water in the reverse micelles. The rate is small at large water concentration, i.e., the rate of disaggregation increases when ω_0 is reduced.

4. Discussion

In this study, we compared the effect of reverse micelles upon either disaggregation or aggregation of three different porphyrins. The amphiphilic character of these porphyrins has already been pointed out in Langmuir film studies.[41] It was found that only the porphyrin of long alkyl chains, PC_{12}, formed stable films with high collapse pressures without any other surfactant additives. In the case of the porphyrin with short alkyl chains (butyl), PC_4, less stable films were formed and none of PC_0. These results show the importance of structural differences in PC_0, PC_4, and PC_{12} self-assembly.

4.1. Porphyrin Solubilization in Reverse Micelles. *At $\omega_0 = 0$.* The stability differences observed in the Langmuir films of aminosulfonylporphyrins reflect directly the hydrocarbon chain length effect on the substitution at the nitrogen atom. Consequently, it is expected that the alkyl chain may affect the solubility of these porphyrins in reverse micelle solutions. Indeed, spectroscopic results showed larger differences between the porphyrins which were all practically insoluble in isooctane. The solubility in this medium increased only if the AOT surfactant was added.

Although experiments with variable AOT concentration were only performed with PC_{12}, we can assume that there is an interaction between all porphyrins and the surfactant. In fact, the solubilization is improved when the concentration of AOT is above the cmc.

The extinction spectra for the porphyrins dissolved in reverse micelles at $\omega_0 = 0$ (Figure 1a–c) show a broadening order for the Soret band $PC_0 > PC_4 > PC_{12}$. Since the broadening is related to the presence of porphyrins' aggregates, the monomer solubility in reverse micelle at $\omega_0 = 0$ increases with the increase of the alkyl chains. Furthermore, the RLS spectra for those solutions (Figure 4, curves 1–3) indicate that the size contribution of aggregates for the scattering follows $PC_0 > PC_4 > PC_{12}$. Based on these results, different types of associated species between the porphyrins and micelles are proposed in Scheme 2.

According to Scheme 2, the porphyrins are dissolved in reverse micelles by forming, I, II, and III aggregates. The main differences between type I and type II aggregates are size and association with micelles, whereas type III aggregates represent the monomer in the reverse micelle.

In the absence of surfactant, alkyl groups can improve the solubility of the large self-aggregates (type I) in isooctane by increasing the porphyrins' polarizability. Thus, we can consider that there is type I aggregate for PC_4 and PC_{12} in isooctane bulk solution but none for PC_0 (without alkyl groups).

Taking into consideration that the PC_{12} extinction spectrum in the $\omega_0 = 0$ solution coincides with the absorption spectrum in acetonitrile solution, this indicates that this porphyrin is probably dissolved to a greater extent in the monomeric form (type III). Also, the PC_4 extinction spectrum in the $\omega_0 = 0$ solution shows similarities with absorption spectrum in acetonitrile, indicating a large proportion of type III. However, due to the broad Soret band base (Figure 1b, curve 1), the presence of type I and II cannot be ruled out. In the case of PC_0, comparison with the absorption spectrum in acetonitrile indicates that there are type II aggregates in the $\omega_0 = 0$ solution.

The fluorescence spectra of porphyrins depend on excitation wavelengths, for instance, excitation at the Soret band in $\omega_0 = 0$ solutions gave emission spectra similar to that of the monomer in acetonitrile solution for all porphyrins. In general, the spectra showed maxima bands around 650 and 720 nm. However, when exciting at either the red edge of the Soret band (~440 nm) or at the Q-band (513 nm) the emission spectra showed the

presence of a red band ∼670 nm with different ratio intensity between ∼650 and ∼670 nm as can be seen for PC$_0$ and PC$_{12}$ in Figure 2, parts a and c, respectively. This phenomenon can be explained by the presence of more than one species that can be responsible for the new red-shift emission band, i.e., dimers or oligomers which are associated to the reverse micelle, in addition to the monomer form as proposed in Scheme 2. The quantification of such species is very difficult because no isosbestic points were detected and, besides, there is the scattering contribution.

The PC$_{12}$ porphyrin in $\omega_0 = 0$ solutions have a fluorescence quantum yield close to the acetonitrile solution which is in agreement with the proposed Scheme 2 where type III aggregates are the main species.

Comparison of extinction and excitation spectra not only gives evidence for the presence of aggregates that are responsible for the emission around 670 nm (type I and/or type II) but also indicates the presence of type III species when the excitation spectra were measured collecting the emission at 650 nm. As shown in Figure 3a−c, spectra 1 for all of the porphyrins show the presence of monomer in the reverse micelle (type III). In addition, the excitation spectrum 2 for PC$_{12}$ (Figure 3c) indicates the presence of type I and/or type II aggregates due to the fluorescence emission at around 670 nm in $\omega_0 = 0$ solutions.

At $\omega_0 \neq 0$. The reverse micelle size and concentration increase and decrease with ω_0, respectively.[35] According to Scheme 2, the type III concentration will be lower than types I and II at low micelle concentration. This is in agreement with the results obtained for PC$_4$ and PC$_{12}$ which contain more type III aggregates than types I and/or II at $\omega_0 = 0$, and this relationship inverts when water is added. In PC$_{12}$, a new extinction band around 376 nm and a red-edge around 450 nm increase when water is added (Figure 1c, curve 1−4). In the corrected absorption spectra, a blue band at 376 nm is still present. Following Scheme 2, the initial type III becomes type II aggregates. In PC$_4$, the same trend occurs with addition of water.

The fluorescence spectra for PC$_4$ and PC$_{12}$ at $\omega_0 = 40$ (spectra 3 in Figure 2, parts b and c) also show that these type II aggregates fluoresce since the emissions were observed upon excitation of the respective new absorption bands which appear in the presence of water in the micellar system. The presence of nonfluorescent aggregates cannot be ruled out; however, since the excitation spectra are narrower than the corresponding extinction spectra. In fact, the absorption spectra extracted from the extinction spectra (Figure 5b) showed sharper bands as observed for the excitation spectra. This is very well demonstrated by the PC$_4$ porphyrin. The excitation spectrum 3 in $\omega_0 = 40$ (Figure 3b) is distinct from the extinction spectrum for the same solution (Figure 1b, curve 4) but similar to the absorption spectrum (Figure 5b). In the excitation and absorption spectra, the 436 nm band is more defined. The RLS spectra also support the increase of type II aggregates in the $\omega_0 \neq 0$ solutions. In Figure 4, the scattering signal is significantly intensified on going from $\omega_0 = 0$ to $\omega_0 = 40$ as shown by spectra 3 and 4 for the PC$_{12}$ porphyrin.

Contrary to the PC$_4$ and PC$_{12}$ results, the solubilization of the nonalkyled PC$_0$ at $\omega_0 \neq 0$ shows that specific interactions should not be ruled out. The extinction and emission spectra of PC$_0$ revealed that the addition of water does not make aggregate type II more significant as in the case of PC$_4$ and PC$_{12}$. Conversely, some type III aggregates seem to be formed. This can be explained by possible hydrogen bonding interactions between PC$_0$ and free water which is present in the interfacial region of reverse micelles. It is known that the amount of free

SCHEME 3
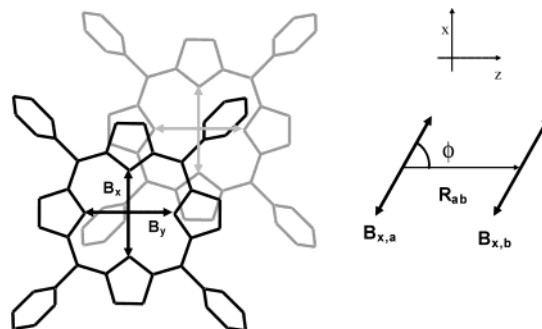
water in this region increases with ω_0 as a sigmoidal function.[48] However, the presence of type III aggregates for PC$_0$ porphyrin is not sufficiently high to significantly change the RLS spectra which still indicate a large presence of type II aggregates.

4.2. Aggregates Morphology. The structure of dye aggregates ranging from dimer to larger oligomers has quite often been described in the literature using the electronic absorption spectroscopic data of the corresponding monomers arrangement. Direct correlation is possible due to the exciton point-dipole coupling theory developed by Kasha et al. in terms of Coulombic interaction between vicinal chromophores.[49−52]

According to the exciton coupling theory, the energy of the electronic transition in the dimer can be interpreted by a combination of the energy of two isolated monomers and the coupling energy, i.e., exciton splitting energy (ΔE) expressed in eq 1

$$\Delta E = \frac{2|\mu_M|^2}{R_{ab}^3}(\cos\Theta - 3\cos\phi_a\cos\phi_b) \qquad (1)$$

This energy is derived from the interactions between transition dipole moments of the two monomers (μ_M) which are dependent on the spatial arrangement as can be seen in Scheme 3.

For J aggregates, the allowed transition is red shifted to the monomer absorption band when the transition dipole moments are "head-to-tail" or "edge-to-edge" (angle between them is $\Theta = 0°$), and they are parallel to the center-to-center distance (R_{ab}), i.e., $\phi_a = \phi_b = 0$ or 180°. Equation 2 gives the relative intensity between the aggregate and monomer. Therefore, the absorption intensity for the J aggregates is 2-fold the intensity of one monomer absorption. The blue shift in the absorption of H-aggregates can also be explained from the exciton theory, since the allowed transition is the "head-to-head" or "face-to-face" arrangement

$$|\mu_\pm|^2 = |\mu_M|^2(1 \pm \cos\Theta) \qquad (2)$$

The theory has been successfully applied to the covalent bond monomer unit.[53] By contrast, it is difficult to access the number of monomers in homoassociated aggregates since the control of the aggregation process is very difficult to obtain and still remains a matter of investigation.

We analyzed our results using the point dipole approximation of exciton theory for the dimer case (see the description for porphyrin in Scheme 3) correlating the spectral shifts with the possible structure. From our data, we assumed that the application of a more sophisticated model would be unnecessary because the coupling energy, which depends on $1/R^3$ (eq 1), falls off strongly with distance.[54] Moreover, the coupling energy for the dimer represents already 50% of the energy for the large array.[53]

Self-Aggregation Process of Lipophilic Porphyrins

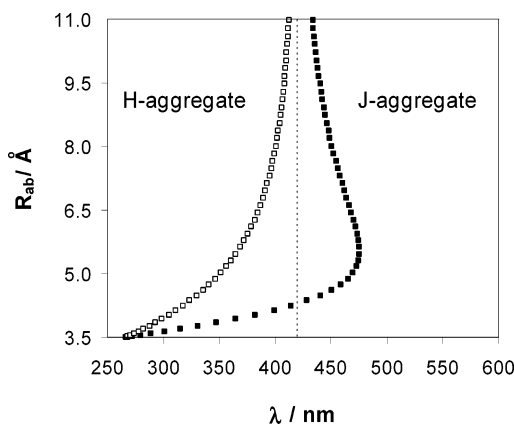*J. Phys. Chem. B, Vol. 108, No. 31, 2004* **11353**

Figure 8. Shifts of allowed transitions in dimer arrangement of two monomers as a function of center-center distance (R_{ab}). The open and close squares correspond to the B_y dipole moments and B_x dipole moments coupling, respectively, as depicted in Scheme 3.

TABLE 2: Geometrical Parameters Describing the Porphyrin Dimers Structures for Corresponding Energy Transition[a]

entry	R_{ab}/Å	r_{offset}/Å	ϕ/degree	λ/nm
1	3.94	1.81	62.7	376
2	4.29	2.48	54.7	419
3	4.49	2.81	51.2	435
4	9.30	8.62	22.1	435
5	4.67	3.09	48.9	445
6	7.62	6.77	27.3	445

[a] See the parameters description in the text.

Here, we built the geometric arrangement for two porphyrins in the dimer based on some experimental observations made by Hunter and Sanders:[11] (i) the porphine cores are coplanar within 3.4−3.6 Å of separation and (ii) the nitrogen−nitrogen axes are parallel between the couple. Furthermore, the porphyrins (D_{2h}) have two orthogonal and (almost) degenerate transition dipole moments, B_x and B_y, resulting in the formation of two degenerate Soret bands.[44] The relative orientation between these transition dipoles in the dimer is usually defined by the high symmetry of the system, that is, C_{2h} or D_{4h} symmetry.[54,55] Therefore, if all of the above assumptions are followed eq 1 can be reduced to the simpler expression where $\phi_a = \phi_b = \phi$.

The PC$_0$ and PC$_4$ porphyrin aggregates at different ω_0 values showed wider absorption bands whose peaks range around 435−446 nm, i.e., corresponding approximately to 1400 cm^{-1} red shift from the respective monomer' Soret band (see Figures 1 and 5). Those red shifts are an indication of J aggregates which can assume the "edge-to-edge" form. Also, a slight shoulder was detected around 400 nm for PC$_4$ or 1100 cm^{-1} blue shift from the Soret band of monomer transition in the presence of reverse micelles and thus the contribution of some H aggregates may be accounted for.

According to the dimer geometry where the interplanar distance (d) is fixed at 3.5 Å (typical value observed in π stacking), the use of eq 1 for the cases where the porphyrin planes are slip planes (see Figure 8) shows that there is just one case when two allowed degenerated high-energy transitions are expected. This happens in the "face-to-face" structure ($\phi = 90°$). The separation between two porphyrin monomers by slipping one of the parallel planes decreases the two allowed transition energies. Just one of them (B_y for instance) corresponds to the coupling of transition dipole moments orthogonal to the center−center vector preserving the transition energy above the monomer transition energy. The other allowed transition comes from the coupling of transition dipole moments (B_x) that are not orthogonal to the center-center vector. The transition energy through this coupling reaches the same values as that of the monomer when $\phi = 54.7°$ and decreases with the slipping movement which makes ϕ smaller than 54.7°. At this stage, the red-shift band should be observed in the dimer spectrum which corresponds to J aggregates. With a further increase of the center−center distance, the coupling responsible for the two transitions decreases until the two monomers dipole transition moments no longer interact. An interesting feature of the coupling is the "inversed parabolic" behavior of the curve

in Figure 8, indicating that for J-aggregate types there are two different set of structures that give the same transition energy.

The spectral shift observed in PC$_0$ ($\sim$445 nm) and PC$_4$ ($\sim$435 nm) porphyrins in the micellar system can be obtained by coupling dipole transition moments[56] for porphyrin−porphyrin interplanar distances of 3.5 Å (Table 2). These particular values give approximately the transition energy for these porphyrins as that observed when comparing Figures 1 and 5. Entries such as 3 and 5 as well as entries 4 and 6 in Table 2 can describe the electronic transitions observed for PC$_0$ and PC$_4$. However, only 4 and 6 entries provide large aggregate structures comparable to that stacking with edge-to-edge profile found in a porphyrin with undecyl side chains, which contains the same Soret band splitting observed here.[57]

The above slipping displacement is greater than the corresponding distance in the TPP crystal lattice.[19] The aminosulfonyl substituents on phenyl in PC$_0$ and PC$_4$ probably cause an additional steric repulsion forcing the porphyrins to move away by slipping the molecular planes. They could also move apart increasing the interplanar distance. This would however reduce the $\pi-\sigma$ attractive interaction.[11] Additionally, the electronic effect due to the electron-acceptor character of the substituent group can induce a larger slipping distance between the porphyrin planes.[18]

Both the corresponding center−center distance and the angle ϕ parameters could explain the spectral shifts for PC$_0$ and PC$_4$, but the intensities for the allowed transitions are not in agreement with those experimentally observed in the extinction spectra. Therefore, a large broadening of the Soret bands probably caused by the inhomogeneity and the size of aggregate structures may lead to an incorrect interpretation.

The approach whereby the scattering contribution was accounted for and the absorption spectrum extracted from the extinction spectrum is very important and can lead to a more correct interpretation. One important feature observed after the correction is the clear intensification of the Q bands mainly for PC$_4$ and PC$_{12}$ in the aggregates forms (Figures 5 and 6). Such behavior was hidden in the corresponding extinction spectra (Figure 1). The increase of Q-band intensity can be explained by the intensity transfer from the strong Soret transition dipole moment due to an exciton coupling that involves the related transition dipoles. In fact, even a weak oscillator strength is enhanced if the energetic distance between the transition bands are not large.[58]

PC$_{12}$ showed more defined and narrow maxima bands; a clearly blue shifted band approximately 2850 cm^{-1} from the monomer Soret band appears in the presence of water in reverse micelles (Figure 1c). Similar cases have been reported, but all of them with more defined splitting in the blue and red regions with almost the same absorption intensities.[13,21,53,59,60] In the case of PC$_{12}$, the band absorption intensity observed for the aggregates (Figures 5 and 6) in the region close to the monomer

transition energy (~421 nm) is larger than the band absorption intensity in the blue region (~376 nm). The presence of the band around 421 nm, assuming that type III are negligible species, indicates that this porphyrin can assume a dimer geometry when the planes are tilted to the center−center vector distance forming an angle close to 54.7°. For d = 3.5 Å, the center−center distance must be 3.9 Å in order that the blue-shift band reaches 376 nm (entry 1 in Table 2). If the interplane distance is increased, all the other parameter must increase to achieve the same transition energy. In general, the geometrical values agree with crystal structure parameters of some aggregates with lipophilic chains substituted in β carbons in the porphine core like 5,15-diphenyl-2,8,12,18-tetra-*n*-hexyl-3,7,-13,17-tetramethyl porphyrin[61]. It was found that the pair of porphyrins is packed within an interplane separation 3.7−4.7 Å and a center-center distance of 6.9−8.8 Å. The orientation of hexyl chains in pairs of porphyrin designs a "chair" shape where the chains are orientated almost parallel. This type of orientation was found also in *meso*-tetra-substituted porphyrins[19,62] similar to the atropisomer *cis*-2,0 in picket fence porphyrins.[25,26] The PC_{12} can assume this type of structure in aggregates since the same chain orientation was also observed for *n*-(*p*-tolyl)-dodecyl sulfonamide structure,[63] but the other types of arrangements cannot be completely ruled out, because of the red-edge observed even after the scattering correction on the absorption correction and the intense RLS signal observed at around 440 nm. Therefore, J aggregates similar to the conformer where all of the 12 carbon chains are on the same side of the porphyrin planes have to be considered. This type of geometry has already been proposed to occur in premicellar J aggregates of picket fence porphyrins with an anionic surfactant (SDS),[25] and it seems the more probable geometry in the monolayer films.[41]

The strong coupling observed for PC_{12} in reverse micelles is related to the additional interactions due to the presence of long alkyl chains in the structure. In the other two porphyrins, such interactions are quite reduced and thus the exciton coupling was minor. In addition, in accordance with the point dipole coupling approach applied to the dimer base model, the PC_{12} planes have to stack more co-facially than other porphyrins as seen by comparing the entries 1 to the 4 and 6 in Table 2. On the other hand, the planes of PC_0 and PC_4 aggregates have greater slip tendencies (larger offset distances).

In particular, PC_{12} aggregates in reverse micelles at high values of ω_0 show the same spectral properties observed in the system in the absence of water but with low concentration of AOT. The PC_{12} and AOT interact to form premicellar aggregates (Figure 6). These premicellar aggregates are large judging from the signal observed in the RLS spectra. However, these premicellar aggregates practically disappear giving monomeric forms when the surfactant concentration is high enough to form the reverse micelle.

Porphyrins are known to form clathrate lattices which can host a large variety of guest molecules with different sizes, where the driving force is the host reordering and demand for more efficient packing. That is, the porphyrins work like "sponges".[62] Therefore, we can speculate that those premicellar aggregates are the AOT surfactant guest in the PC_{12} type of crystal whose size is enough to scatter the incident light. The increase of AOT concentration in the PC_{12} crystal can increase the repulsion between the lateral chains enhancing solubilization of the monomer at high AOT concentration.

4.3. Reverse Micelle/Porphyrin Aggregation Kinetic. The aggregation mechanism of porphyrins has been studied as a growth process which starts from a low number of homoassociated species and increases until colloidal sizes are achieved, i.e., the mechanism should involve the initial formation of dimers, trimers, tetramers, and so on.

There are few studies on this particular issue which involve porphyrins. In fact, kinetic studies of aggregation have been successfully applied in positively charged water soluble porphyrins by either reaction-limited aggregation (RLA) or diffusion-limited aggregation DLA.[64−66] More recently, Pasternack et al. has observed that the protonated TSPP aggregation follows an autocatalytic pathway.[65] Although the quantification of this mechanism is being developed, we can give an overview of the process which involves the interaction between the porphyrins and the reverse micelle. An important remark should be made about the scattering contribution in the aggregation kinetic traces observed for PC_{12}. As mentioned above, the porphyrins in the reverse micelle show scattering contributions that have to be discounted from the extinction spectra in order to obtain the "true" absorption spectra. However, this is done by the use of RLS spectra obtained in a different instrument. Unfortunately, following the decrease of porphyrin monomer by the light reduction at the Soret wavelength in time evolution, such correction cannot be employed. Therefore, the kinetic traces obtained have, besides the monomer's absorption decrease, the increase of scattering signal. However, for a qualitative analysis, we can assume that scattering contribution at monomer Soret band absorption is not important (see the scattering curve in Figure 5a); the extinction values from the kinetic traces can be seen as the absorption values. This approximation is valid for the early times in the traces. For the long times, the scattering contribution might be larger.

During the process of porphyrin aggregation, the system has to involve different numbers and sizes of aggregates. Thus, the rate constant observed for the PC_{12} aggregation in micellar system should increase with porphyrin concentration. Indeed, this is observed (Figure 7). The concentration effect can be achieved either by adding more porphyrin or reducing the reverse micelle concentration. The interesting fact is that the process needs an "induction period" probably to accumulate a number of small aggregates. This "induction period" also depends on the porphyrin and micelle concentrations. The micelle concentration at ω_0 = 5 is approximately 2.5-fold higher than the solution with ω_0 = 10. The average occupation number of porphyrin in ω_0 = 5 at a concentration of 3.0 μM does not differ much from the average occupation number of PC_{12} with 1.5 μM concentration in ω_0 = 10 and thus cannot justify the large difference between the aggregation in both systems (see Figure 7b). Thus, another effect must be involved. The solubilization of water in reverse micelles, aforesaid, contributes to the increase of the micelle size. In addition, the PC_{12} porphyrin is dissolved in the micelle probably in the interfacial region which can laterally diffuse. If the aggregation must start with a small association, e.g., the dimer can be formed by collision of two micelles occupied by the monomers, thus the presence of more than one monomer that can freely diffuse to start the growth should occur in the same micelle. In ω_0 = 10, the surfactant heads are more hydrated than in ω_0 = 5 and there are free water molecules in the so-called hydrophobic part in the interfacial region.[48] Thus, PC_{12} in this region is free to diffuse, given the hydrophobic effect caused by the free water. This effect pushes the porphyrin outward through the reverse micelle interface exposing the molecule to association. At low ω_0, like at [water]/[AOT] = 5, the porphyrin can be better sustained and the structure is less inclined to more aggregation.

Self-Aggregation Process of Lipophilic Porphyrins

J. Phys. Chem. B, Vol. 108, No. 31, 2004 **11355**

After the "induction period", the aggregation rates reach maxima values and then the reaction slows down. The porphyrin aggregation growth is related to the formation of small aggregates and these from their formation from smaller ones and so on. The process of this sequence is based on the size of the starting molecule. In fact, the growth mechanism in fractal aggregates relates the aggregate mass M to the corresponding radius R by a scaling form $M \propto R^{d_f}$ where d_f is related to the fractal dimension.[64-66] Nevertheless, our results are very similar to those of Pasternack et al. on the protonated TSPP aggregation kinetics.[65] Their results show that prenuclear species which are formed fast work as "seed" for the aggregation. Also, they followed the reaction at the two wavelengths: 435 nm for the monomer absorption band and 490 nm for the J aggregate with a large contribution of the scattering signal. The only differences observed are related to the evolution of that aggregation pathway which depended on initial conditions and the size parameters. Therefore, we can assume that the aggregation rates are related to the size and quantity of the previous small aggregates or "pre-aggregates". However, it seems that the aggregates cannot grow to infinite size which means that once a determined size is achieved the process rates decrease. Then, on one hand, there is a balance between the noncovalent interactions which keep the monomers and surfactant molecules associated and on the other the medium polarity. It may, then, be possible to control the size of such aggregates by changing the surfactant and/or medium polarity. A more detailed quantitative analysis of the dynamics of the PC_{12} aggregation is underway.

5. Conclusion

The presence of alkyl substitution and water strongly determine the solubilization and the aggregation kinetics in the micelles and the spectroscopic features of the system. At $\omega_0 = 0$, only the porphyrin PC_{12} is dissolved in the monomeric form and dispersed in the interfacial micellar region, whereas PC_0 is present basically in the form of nonspecific and J aggregates. PC_4 porphyrins are partially dissolved as monomers in reverse micelles. At $\omega_0 \neq 0$, the PC_4 porphyrin monomers are definitively less concentrated than the nonspecific and J aggregates. The PC_{12} monomer concentration is also reduced with the increase of H and J aggregates. By contrast, PC_0 monomer porphyrin concentration is increased in the presence of water which indicates the importance of hydrogen bonding in the solubilization process. The scattering contribution was accounted to extract the "true" absorption spectra from the experimental extinction spectra. A better definition of the Soret band region was observed, but no significant changes in the peak positions were observed after the corrections. From point dipole exciton theory, the spectral features of Soret bands show that the structures can also be dependent on the chain length. PC_0 and PC_4 are present as J aggregates with the porphyrin planes slipper than in the tetraphenylporphyrin lattice crystal, whereas in PC_{12} aggregates, the porphyrins are stacked in a more co-facial structure; thus, the structures of H aggregates are likely to be present. However, due to the larger RLS signal at red spectral region the presence of J aggregates cannot be disregarded as the other type of geometrical conformer. The PC_{12} porphyrin seems to aggregate by an autocatalytic process which depends on the size parameter of initial "pre-aggregates".

Note Added after ASAP Posting. This article was released ASAP on 6/30/2004. Sentence 4 in the Conclusion Section was revised. The correct version was posted on 7/12/2004.

References and Notes

(1) Wasielewski, M. R. *Chem. Rev.* **1992**, *92*, 435.

(2) Hayashi, T.; Ogoshi, H. *Chem. Soc. Rev.* **1997**, *26*, 355.

(3) Tran-Thi, T.-H. *Coord. Chem. Rev.* **1997**, *160*, 53.

(4) Purrelo, R.; Gurrieri, S.; Luceri, R. *Coord. Chem. Rev.* **1999**, *190−192*, 683.

(5) Boyle, R. W.; Dolphin, D. *Photochem. Photobiol.* **1996**, *64*, 469.

(6) Kalyanasundaram, K.; Grätzel, M. *Coord. Chem. Rev.* **1998**, *77*, 347.

(7) Aziz, A.; Narasimhan, K. L.; Periasamy, N.; Maiti, N. C. *Philosoph. Magn. B* **1999**, *79*, 993.

(8) Feiters, M. C.; Rowan, A. E.; Nolte, R. J. M. *Chem. Soc. Rev.* **2000**, *29*, 375.

(9) Pullerits, T.; Sundström, V. *Acc. Chem. Res.* **1996**, *29*, 381.

(10) Müller-Dethlefs, K.; Hobza, P. *Chem. Rev.* **2000**, *100*, 143.

(11) Hunter, C. A.; Sanders, J. K. M. *J. Am. Chem. Soc.* **1990**, *112*, 5525.

(12) Menger, F. M. *Proc. Natl. Acad. Sci.* **2002**, *99*, 4818.

(13) Siggel, U.; Bindig, U.; Endisch, E.; Komatsu, T.; Tsuchida, E.; Voigt, J.; Fuhrhop, J.-H. *Ber. Bunsen-Ges. Phys. Chem.* **1996**, *100*, 2070.

(14) Shirakawa, M.; Kawano, S.-I.; Fujita, N.; Sada, K.; Shinkai, S. *J. Org. Chem.* **2003**, *68*, 5037.

(15) Komatsu, T.; Moritake, M.; Nakagawa, A.; Tsuchida, E. *Chem. Eur. J.* **2002**, *8*, 5469.

(16) Scolaro, L. M.; Castriaciano, M.; Romeo, A.; Patanè, S.; Cefalì, E.; Allegrini, M. *J. Phys. Chem. B* **2002**, *106*, 2453.

(17) Komatsu, T.; Tsuchida, E.; Böttcher, C.; Donner, D.; Messerschmidt, C.; Siggel, U.; Stocker, W.; Rabe, J. P.; Fuhrhop, J.-H. *J. Am. Chem. Soc.* **1997**, *119*, 11660.

(18) Okada, S.; Segawa, H. *J. Am. Chem. Soc.* **2003**, *125*, 2792.

(19) Kano, K.; Fukuda, K.; Wakami, H.; Nishiyabu, R.; Pasternack, R. F. *J. Am. Chem. Soc.* **2000**, *122*, 7494.

(20) Choi, M. Y.; Pollard, J. A.; Webb, M. A.; McHale, J. L. *J. Am. Chem. Soc.* **2003**, *125*, 810.

(21) Kubát, P.; Lang, K.; Procházková, K.; Anzenbacher, P., Jr. *Langmuir* **2003**, *19*, 422.

(22) Akins, D. L.; Zhu, H.-R.; Guo, C. *J. Phys. Chem.* **1996**, *100*, 5420.

(23) Maiti, N. C.; Mazumdar, S.; Periasamy, N. *J. Phys. Chem. B* **1998**, *102*, 1528.

(24) Agostiano, A.; Catucci, L.; Colafemmina, G.; Scheer, H. *J. Phys. Chem. B* **2002**, *106*, 1446.

(25) Barber, D. C.; Woodhouse, T. E.; Whitten, D. G. *J. Phys. Chem.* **1992**, *96*, 6, 5106.

(26) Barber, D. C.; Freitag-Beeston, R. A.; Whitten, D. G. *J. Phys. Chem.* **1991**, *95*, 4074.

(27) Gandini, S. C. M.; Yushmanov, V. E.; Borissevitch, I. E.; Tabak, M. *Langmuir* **1999**, *15*, 6233.

(28) Borovkov, V. V.; Anikin, M.; Wasa, K.; Sakata, Y. *Photochem. Photobiol.* **1996**, *63*, 477.

(29) Menger, F. M.; Caran, K. L.; Seredyuk, V. A. *Angew. Chem., Int. Ed.* **2001**, *40*, 3905.

(30) Andrade, S. M.; Costa, S. M. B. *Biophys. J.* **2002**, *82*, 1607.

(31) Paulo, P. M. R.; Costa, S. M. B. *Photochem. Photobiol. Sci.* **2003**, *2*, 597.

(32) Prieto, I.; Pedrosa, J. M.; Martín-Romero, M. T.; Möbius, D.; Camacho, L. *J. Phys. Chem. B* **2000**, *104*, 9966.

(33) Gonsalves da Silva, A. M.; Viseu, M. I.; Malathi, A.; Antunes, P.; Costa, S. M. B. *Langmuir* **2000**, *16*, 1196.

(34) (a) Kasha, M.; Rawls, H. R.; El-Bayoumi, M. A. *Pure. Appl. Chem.* **1965**, *11*, 371. (b) McRae, E. G.; Kasha, M. in *Physical Processes in Radiation Biology*; Academic Press: New York, 1964; p 23.

(35) Luisi, P. L.; Giomini, M.; Pileni, M. P.; Robinson, B. H. *Biochim. Biophys. Acta* **1988**, *947*, 209.

(36) Costa, S. M. B.; Lopez-Cornejo, P.; Togashi, D. M.; Laia, C. A. T. *J. Photochem. Photobiol. A* **2001**, *142*, 151.

(37) Silber, J. J.; Falcone, R. D.; Correa, N. M.; Biasutti, M. A.; Abuin, E.; Lissi, E.; Campodonico, P. *Langmuir* **2003**, *19*, 2067.

(38) Raju, B. B.; Costa, S. M. B. *J. Phys. Chem. B* **1999**, *103*, 4309.

(39) Tatikolov, A. S.; Costa, S. M. B. *Chem. Phys. Lett.* **2001**, *346*, 233.

(40) (a) Micali, N.; Mallamace, F.; Castriciano, M.; Romeo, A.; Scolaro, L. M. *Anal. Chem.* **2001**, *73*, 4958. (b) Collings, P. J.; Gibbs, E. J.; Starr, T. E.; Vafek, O.; Yee, C.; Pomerance, L. A.; Pasternack, R. F. *J. Phys. Chem. B* **1999**, *103*, 8474.

(41) Hudson, A. J.; Richardson, T.; Thirtle, J. P.; Roberts, G.; Johnstone, R. A. W.; Sobral, A. J. F. N. *Mol. Cryst. Liq. Cryst.* **1993**, *235*, 103.

(42) Harriman, A.; Hosie, R. J. *J. Chem. Soc., Faraday Trans. 2* **1981**, *77*, 1695.

(43) Togashi, D. M.; Costa, S. M. B.; Sobral, J. F. N.; Gonsalves, A. M. d'A. R. *Chem. Phys.* **2004**, *300*, 267.

(44) Gouterman, M. In *The Porphyrins*; Dolphin, D., Ed.; Academic Press: New York, 1978; Vol. 3, Chapter 1, pp 1−165.

(45) PC_{12} very little soluble.

(46) (a) Pasternack, R. F.; Bustamante, C.; Collings, P. J.; Giannetto, A.; Gibbs, E. J. *J. Am. Chem. Soc.* **1993**, *115*, 5393. (b) Pasternack, R. F.; Schaefer, K. F. *Inorg. Chem.* **1994**, *33*, 2062. (c) Pasternack, R. F.; Collings, P. J. *Science* **1995**, *269*, 935. (d) Parkash, J.; Robblee, J. H.; Agnew, J.; Gibbs, E.; Collings, P.; Pasternack, R. F.; de Paula, J. C. *Biophys. J.* **1998**, *74*, 2089.

(47) (a) Majhi, P. R.; Moulik, S. P. *J. Phys. Chem. B* **1999**, *103*, 5977. (b) Manoj, K. M.; Jayakumar, R.; Rakshit, S. K. *Langmuir* **1996**, *12*, 4048. (c) Muto, S.; Meguro, K. *Bull. Chem. Soc. Jpn.* **1973**, *46*, 1316.

(48) Laia, C. A. T.; Costa, S. B. M. *J. Chem. Soc., Faraday Trans.* **1998**, *94*, 2367.

(49) Czikkeley, V.; Föterling, H. D.; Kuhn, H. *Chem. Phys. Lett.* **1970**, *6*, 207−210.

(50) Hochstrasser, R. M.; Kasha, M. *Photochem. Photobiol.* **1964**, *3*, 317.

(51) Hunter, C. A.; Sanders, J. K. M.; Stone, A. J. *Chem. Phys.* **1989**, *133*, 395.

(52) Knapp, E. W. *Chem. Phys.* **1984**, *85*, 73.

(53) Aratani, N.; Osuka, A.; Cho, H. S.; Kim, D. *J. Photochem. Photobiol. C* **2002**, *3*, 25.

(54) Ribó, J. M.; Bofill, J. M.; Crusats, J.; Rubires, R. *Chem. Eur. J.* **2001**, *7*, 2733.

(55) Gouterman, M.; Holten, D.; Lieberman, E. *Chem. Phys.* **1977**, *25*, 139.

(56) The transition dipole moment used for the calculations were obtained by integration of the absorption band of PC_{12} at $\omega_0 = 0$ that is approximately equal to 9.5 D. The Soret transition wavelength is equal to 419 nm, on average.

(57) Balaban, T. S.; Eichhöfer, A.; Lehn, J.-M. *Eur. J. Org. Chem.* **2000**, 4047.

(58) Zimmermann, J.; Siggel, U.; Fuhrhop, J.-H.; Röder, B. *Phys. Chem. B* **2003**, *107*, 6019.

(59) Schell, C.; Hombrecher, H. K. *Chem. Eur. J.* **1999**, *5*, 587.

(60) Fuhrhop, J.-H.; Demoulin, C.; Boettcher, C.; Köning, J.; Siggel, U. *J. Am. Chem. Soc.* **1992**, *114*, 4159.

(61) Bond, A. D.; Feeder, N.; Redman, J. E.; Teat, S. J.; Sanders, J. K. M. *Cryst. Growth Des.* **2002**, *2*, 27.

(62) Byrn, M. P.; Curtis, C. J.; Hsiou, Y.; Khan, S. I.; Sawin, P. A.; Tendick, S. K.; Terzis, A.; Strouse, C. E. *J. Am. Chem. Soc.* **1993**, *115*, 9480.

(63) Rajeswaran, M.; Blanton, T. N.; Zumbulyadis, N.; Giesen, D. J.; Conesa-Moratilla, C.; Misture, S. T.; Stephens, P. W.; Huq, A. *J. Am. Chem. Soc.* **2002**, *124*, 14450.

(64) Micali, N.; Mallamace, F.; Romeo, A.; Purrello, R.; Scolaro, L. M. *J. Phys. Chem. B* **2000**, *104*, 5897.

(65) Pasternack, R. F.; Fleming, C.; Herring, S.; Collings, P. J.; dePaula, J.; DeCastro, G.; Gibbs, E. J. *Biophys. J.* **2000**, *79*, 550.

(66) Mallamace, F.; Micali, N.; Trusso, S.; Scolaro, L. M.; Romeo, A.; Terracina, A.; Pasternack, R. F. *Phys. Rev. Lett.* **1996**, *76*, 4741.